Preparation, crystal structure, and reducibility of K_2NiF_4 type oxides $Sm_{2-x}Sr_xNiO_{4+\delta}$

Hui Lou,*[a] Yuping Ge,[a] Ping Chen,[a] Minghua Mei,[a] Futai Ma[a] and Guanglie Lü[b]

[a]*Department of Chemistry, Hangzhou University, Hangzhou 310028, China*
[b]*Central Laboratory, Hangzhou University, Hangzhou 310028, China*

K_2NiF_4 type compounds $Sm_{2-x}Sr_xNiO_{4+\delta}$ ($0.4 \leqslant x \leqslant 1.2$) have been synthesized by a citric acid complex decomposition method. Rietveld refinement of the powder X-ray diffraction data showed that there was a crystal system transformation from orthorhombic *Fmmm* to tetragonal *I*4/*mmm* at around $x = 0.6$. The Sr substitution caused a drastic shift of the O_{II} ions along the *c* axis from Sm(Sr) towards Ni whilst scarcely affecting the NiO_4 network in the basal plane. The distortion of the NiO_6 octahedron decreased, while the average bond valence of Ni increased with increasing *x*.

K_2NiF_4 type rare-earth complex oxides, A_2BO_4, consist of alternating layers of ABO_3 perovskite and AO rock-salt structures along the *c*-axis.[1–3] They were widely studied owing to their high temperature stability, two-dimensional conductivity, antiferromagnetic properties, semiconductor–metal transition properties and superconductivity.[1–5] These properties are closely related to the types of the ions A and B, interatomic distances in the crystal, and the valence state of the transition-metal ions B which can be altered by substitution of other ions such as Sr^{2+} for A.[6,7] It is necessary to determine precise crystal structures so as to further understand the relationships between properties and the crystal structure. The Rietveld method, a profile refinement method of analyzing X-ray powder diffraction data by fitting the entire diffraction pattern to a calculated one, has been widely used to refine crystal structure.[8] Recently, an application of the Rietveld method to refine the crystal structure of $La_{2-x}Sr_xNiO_4$ and $Nd_{2-x}Sr_xNiO_4$ has been reported.[9–11]

A tolerance factor, *t*, is usually used to predict the possibility of K_2NiF_4 structure formation. Ganguli[12] proposed a criterion according to which the tetragonal structure is stable when the tolerance factor, ($t = r_A/r_B$), lies between 1.7 and 2.4. Because of the limitation of the tolerance factor, neodymium is the smallest rare earth metal ion forming a K_2NiF_4 type lanthanide nickelate.[11] Samarium, which is smaller than Nd, can not form nickelate compounds with the K_2NiF_4 type structure. By partial substitution of Sr^{2+} for Sm^{3+}, however, K_2NiF_4 type compounds $Sm_{2-x}Sr_xNiO_{4+\delta}$ can also be prepared. In this study, we prepared $Sm_{2-x}Sr_xNiO_{4+\delta}$ ($0.4 \leqslant x \leqslant 1.2$), refined their crystal structure by X-ray Rietveld analysis, and measured their IR spectra and reducibility. The effects of Sr substitution on the structural parameters are discussed.

Experimental

Preparation

$Sm_{2-x}Sr_xNiO_{4+\delta}$ ($x = 0$, 0.2, 0.4, 0.5, 0.6, 0.8, 1.0, 1.2, 1.4, 1.6) samples were prepared by evaporating aqueous solutions of the mixed metal nitrates containing an equivalent amount of citric acid to obtain a gel, followed by decomposion at 920 K for 4 h. Samples were then ground, pelletized and calcined in air at 1473 K for 10 h.

Composition determination

The metal-ion composition was determined by inductively coupled plasma spectrometry (ICP) (USA Leeman, Plasma Spec I).

Crystal structure characterization

XRD data for Rietveld refinement were collected on a Rigaku D/max-3B powder diffractometer with Bragg–Brentano geometry using graphite-monochromated Cu-Kα radiation (40 kV × 30 mA) and a scintillation detector. The intensity data were collected at 25 °C over a 2θ range 10–130° with a step interval of 0.02° and a counting time of 8 s per step. The *d* spacings were corrected for systematic errors by calibration with standard silicon powder ($a = 0.543\,09$ nm). The Rietveld structure refinement was performed using the program WYRLET (M. Schneider, a modified version of the program by Wiles and Young, 1981).[13] The starting model used in the refinement was the space group *Fmmm* or *I*4/*mmm* with structural parameters of a K_2NiF_4 type compound. Peaks were modeled using the pseudo-Voigt profile function in which a peak asymmetry parameter was included for peaks up to $2\theta = 50°$. The background parameters were modeled using a refinable fourth-order polynomial. The occupation number of atoms for all sites were fixed and were not refined. Table 1 lists the variables and the number of these in the refinement.

Determination of Ni^{3+} content

The percentage Ni^{3+} content, relative to the total nickel in the sample, was determined iodometrically according to the method described in ref. 6 and 14. In a three-necked spherical flask kept under an N_2 flow and containing 30 cm^3 of 0.5 mol dm^{-3} HCl and 600 mg of KI (both in excess), *ca.* 150 mg of accurately weighed sample was added and the flask was kept in the dark for *ca.* 5 min. After dissolution of the solid, the solution was quickly titrated with 0.01 mol dm^{-3} $Na_2S_2O_3$. From the values of the mean oxidation number, the percentage

Table 1 Parameters and number of parameters in the refinement

parameters	number
zero-point parameter	1
background coefficients	5
scale factor parameter	1
fractional atomic coordinates	2
isotropic thermal parameters	4
FWHM parameters	3
cell constants	2 for *I*4/*mmm*, 3 for *Fmmm*
asymmetry parameter	1
mixing parameter	1
preferred orientation parameter	1
total parameters	21 for *I*4/*mmm*, 22 for *Fmmm*

Table 2 The mass% of Sm, Sr and Ni ions and compositions in $Sm_{2-x}Sr_xNiO_{4+\delta}$ determined by ICP (data in parentheses are calculated values)

x	Sm	Sr	Ni	composition[a]
0.4	60.39(60.40)	9.05(8.80)	15.02(14.73)	$Sm_{1.59}Sr_{0.41}Ni^{2+}{}_{0.55}Ni^{3+}{}_{0.45}O_{4.02}$
0.5	57.06(57.53)	11.60(11.17)	15.09(14.97)	$Sm_{1.48}Sr_{0.52}Ni^{2+}{}_{0.47}Ni^{3+}{}_{0.53}O_{4.01}$
0.6	54.43(54.57)	13.84(13.63)	15.49(15.21)	$Sm_{1.39}Sr_{0.61}Ni^{2+}{}_{0.37}Ni^{3+}{}_{0.63}O_{4.01}$
0.8	48.42(48.35)	18.68(18.78)	15.58(15.73)	$Sm_{1.20}Sr_{0.80}Ni^{2+}{}_{0.17}Ni^{3+}{}_{0.83}O_{4.02}$
1.0	41.93(41.69)	24.55(24.29)	16.45(16.27)	$Sm_{1.00}Sr_{1.00}Ni^{2+}{}_{0}Ni^{3+}{}_{1.00}O_{4.01}$
1.2	34.80(34.56)	30.45(30.20)	16.59(16.86)	$Sm_{0.80}Sr_{1.20}Ni^{2+}{}_{0}Ni^{3+}{}_{1.00}O_{3.97}$

[a]The contents of Ni^{2+},Ni^{3+} and oxygen were calculated from the mean oxidation number of Ni, as measured by iodometry.

of Ni^{3+} in the sample was readily calculated and values are given in Table 2.

IR measurements

The IR spectra were taken with a Pekin-Elmer 683 spectrophotometer. Samples were produced in the form of KBr pellets.

Temperature-programmed reduction (TPR) experiments

Samples of $Sm_{2-x}Sr_xNiO_{4+\delta}$ (*ca.* 5 mg) were placed in a quartz reactor which was connected to a conventional TPR apparatus.[15] In order to eliminate any possible contamination, samples were first pretreated with oxygen (flow rate 30 ml min^{-1}) to 1073 K at 20 K min^{-1} for 15 min, and then cooled to room temperature in flowing oxygen. The reduction gas employed was 10% (v/v) hydrogen in nitrogen (flow rate 20 ml min^{-1}). After flushing, the reactor was heated to the final temperature (1173 K) at 20 ml min^{-1}.

Results and Discussion

Compositions and phases of $Sm_{2-x}Sr_xNiO_{4+\delta}$

Table 2 lists the compositions of the compounds as measured by ICP. It can be seen that the results do not deviate significantly from the starting compositions. Table 3 lists the phase characterization results of $Sm_{2-x}Sr_xNiO_{4+\delta}$ obtained from XRD. The single-phase K_2NiF_4 type compounds were obtained within the Sr^{2+} substitution range from $x=0.4$ to 1.2. Because of the limitation of the tolerance factor ($t=r_A/r_B$), the K_2NiF_4 type structure compounds can only be produced for t within the range 1.7–2.4. According to the values of the tolerance factor based on Shannon's ionic radii[16] (listed in Table 4), neodymium is the smallest rare earth metal which can form a K_2NiF_4 type lanthanide nickelate Nd_2NiO_4. Since Sm is smaller than Nd, it can not form a K_2NiF_4 type compound. It is possible, however, for Sm to form K_2NiF_4 type compounds $Sm_{2-x}Sr_xNiO_{4+\delta}$ by partial substitution of alkaline-earth metals (A) with larger ionic radii which increases r_A, or by oxidizing B ions to a higher valence state to decrease r_B. For $x=0.2$, Sr^{2+} substitution is not sufficient to incorporate all the Sm^{3+} and Ni^{2+} into the K_2NiF_4 type structure and some Sm_2O_3 and NiO remain as separate phases (Table 3). When Sr^{2+} substitution is >1.4, monophase samples can not be obtained owing to geometric factors and the charge balance considerations: the excess of Sr and Ni remain as $SrCO_3$ and NiO, respectively.

Structure of $Sm_{2-x}Sr_xNiO_{4+\delta}$ ($0.4 \leqslant x \leqslant 1.2$)

The powder X-ray diffraction patterns of the samples can be indexed based on orthorhombic symmetry with space group *Fmmm* ($x=0.4$–0.6) and tetragonal symmetry with space group *I*4/*mmm* ($x=0.8$–1.2). The agreement between the observed and calculated powder X-ray diffraction profiles of one sample in the final refinement is shown in Fig. 1.

Table 4 Values of the tolerance factor ($t=r_A/r_B$) of Nd^{2+}, Sm^{3+} and Sr^{2+} with different valence values of Ni ions based on Shannon's ionic radii

	Nd^{2+}	Sm^{3+}	Sr^{2+}
Ni^{2+}	1.69	1.64	1.90
Ni^{3+} (low spin)	2.08	2.02	2.30
Ni^{3+} (high spin)	1.94	1.89	2.20

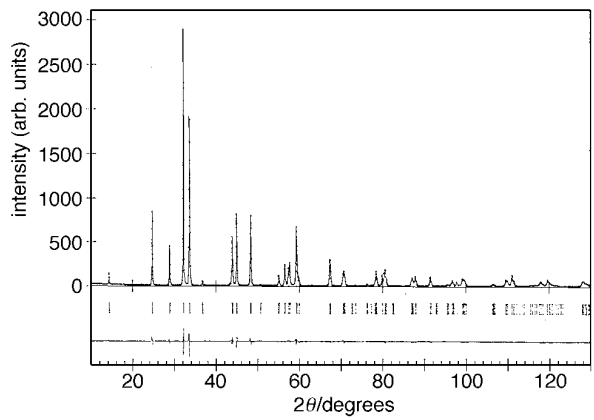

Fig. 1 Rietveld refinement patterns for $Sm_{1.4}Sr_{0.6}NiO_{4+\delta}$. The observed data are indicated by dots and the calculated by the solid line overlaying them. The short vertical lines mark the positions of possible Bragg reflections and the lower curve shows the difference between the observed and calculated powder diffraction patterns.

Table 3 Crystallographic characterization of $Sm_{2-x}Sr_xNiO_{4+\delta}$

x	phase composition	a/Å	b/Å	c/Å	space group
0.0	Sm_2O_3, NiO				
0.2	Sm_2O_3, NiO, $Sm_{2-x}Sr_xNiO_{4+\delta}(0.2 \leqslant x \leqslant 0.4)$				
0.4	$Sm_{1.6}Sr_{0.4}NiO_{4+\delta}$	5.3356(1)	5.3588(1)	12.3014(2)	*Fmmm*
0.5	$Sm_{1.5}Sr_{0.5}NiO_{4+\delta}$	5.3103(1)	5.3534(1)	12.3415(2)	*Fmmm*
0.6	$Sm_{1.4}Sr_{0.6}NiO_{4+\delta}$	5.3257(1)	5.3172(1)	12.3471(1)	*Fmmm*
0.8	$Sm_{1.2}Sr_{0.8}NiO_{4+\delta}$	3.7727(1)		12.2795(2)	*I*4/*mmm*
1.0	$Sm_{1.0}Sr_{1.0}NiO_{4+\delta}$	3.7844(1)		12.2230(2)	*I*4/*mmm*
1.2	$Sm_{0.8}Sr_{1.2}NiO_{4+\delta}$	3.7922(1)		12.2017(1)	*I*4/*mmm*
1.4	$Sm_{2-x}Sr_xNiO_{4+\delta}(1.2<x<1.4)$, $SrCO_3$				
1.6	$Sm_{2-x}Sr_xNiO_{4+\delta}(1.2<x<1.6)$, $SrCO_3$, NiO				

The lattice parameters a, b and c obtained are listed in Table 3. With increasing x, c reached a maximum in the range $0.5 \leqslant x \leqslant 0.6$, similar to the systems $La_{2-x}Sr_xNiO_4$[10] and $Nd_{2-x}Sr_xNiO_4$.[11] As indicated in Table 3 there is a crystal system transformation at x *ca.* 0.6.

Tables 5 and 6 list structural parameters and interatomic distances for the $Sm_{2-x}Sr_xNiO_{4+\delta}$ system. From Table 6, it can be seen that the bond length of Ni—O_I ($\parallel a$-axis) varies similarly to a and b parameters with increasing x, and interatomic distance Sm(Sr)—Sm(Sr) ($\parallel c$-axis) and Sm(Sr)—Ni ($\parallel c$-axis) vary similarly to the parameter c. It is of substantial interest that the Ni—O bond length ($\parallel c$-axis) monotonously decreases with increasing x without exhibiting any anomaly at $x = 0.5$–0.6 as expected from the variation of the parameter c, which indicates that the distortion of NiO_6 octahedra along the c-axis monotonously decreases with increasing x. This can also be confirmed by the bond length ratio of Ni–O_{II} ($\parallel c$-axis) to NiO_I ($\parallel a$-axis) as shown in Table 6. The % bond length change, Δ, defined as $(d_{max} - d_{min})/d_{min}$, within the range $0.4 \leqslant x \leqslant 1.2$, was used to clarify the extent of variation of interatomic distances, as shown in Table 6. The data can roughly be divided into two regions. In the first region Δ values for Ni—O_I ($\parallel a$-axis), Sm(Sr)—O_I, Sm(Sr)—Sm(Sr)($\parallel c$-axis) and Sm(Sr)—Ni($\parallel c$-axis) are all around 1%, whereas in the second region Δ for Ni—O_{II} ($\parallel c$-axis) and Sm(Sr)—O_{II} ($\parallel c$-axis), are above 5%. This indicates that there is a rigid NiO_4 network parallel to the a,b plane which is affected very little by Sr substitution whereas Sr substitution causes a drastic shift of the O_{II} ions from Sm(Sr) sites to Ni while the unit-cell dimensions remain essentially unaltered.

The shift of the O_{II} ions from Sm(Sr) towards Ni may arise for two reasons. On the one hand, the bond strength of M—O can be presented in terms of the sum of the M—O bond formation enthalpies $\Sigma(\Delta H_{M-O})$ in the solids[17] and Table 7 lists calculated results. It can be seen that $\Sigma(\Delta H_{A-O})$ decreases with increasing x, which indicates that the acidity of the A ions decreases and the strength of A—O bond reduces with substitution by Sr. On the other hand, after Sr^{2+} partially substitutes for Sm^{3+}, some Ni^{2+} ions are oxidized to Ni^{3+} in order to meet charge balance considerations. The acidity of the B ion then decreases, and its bond to oxygen becomes stronger. A combination of these effects causes O_{II} to shift from Sm(Sr) towards Ni ions.

According to Pauling's principles of bond valence,[18] the average bond valence of Ni, $S = (R/R_1)^{-N}$, which has a close relationship to the bond lengths in inorganic crystals, can be calculated and results are listed in Table 7, where R is the bond length of Ni—O_I or Ni—O_{II}, R_1 the length expected for a bond of unit valence and N is an empirical constant. For Ni^{2+} $R_1 = 1.680$ and $N = 5.4$. Fig. 2 shows that the average bond valence of Ni increases linearly with increasing x in the $Sm_{2-x}Sr_xNiO_{4+\delta}$ system. The straight line has a break at $x = 0.6$, which is in accord with the fact that there is a crystal system transformation at x *ca.* 0.6.

IR spectra of $Sm_{2-x}Sr_xNiO_{4+\delta}$ are shown in Fig. 3. There are three main absorption bands at *ca.* 700, 520 and 400 cm^{-1}, which are assigned to the symmetric stretching of Sm(Sr)—O_{II}—Ni ($\parallel c$-axis), asymmetric stretching, and bending modes of the Ni—O_I linkages in the basal planes, respectively.[19] All the absorption bands become weaker with increased x, consistent with the decrease of the distortion of NiO_6 octahedra and the increase of symmetry of the crystal structure, as discussed above.

Table 5 Positional and thermal parameters for $Sm_{2-x}Sr_xNiO_{4+\delta}$

atom	site		$x = 0.4$	$x = 0.5$	$x = 0.6$
Sm, Sr	8*i*	z	0.3604(1)	0.3604(1)	0.3603(1)
		B/Å^2	0.74(2)	0.64(2)	0.52(2)
Ni	4*a*	B/Å^2	0.19(7)	0.35(6)	0.28(5)
O_I	8*e*	B/Å^2	1.63(24)	1.34(22)	0.54(16)
O_{II}	8*i*	z	0.1756(5)	0.1738(5)	0.1716(4)
		B/Å^2	2.76(26)	1.92(21)	1.96(17)
		R_{wp}	11.62	11.49	10.11
residuals(%)		R_p	8.36	8.32	7.33
		R_e	0.72	0.72	0.65
		R_i	3.18	3.26	2.45
	site		$x = 0.8$	$x = 1.0$	$x = 1.2$
Sm, Sr	4*e*	z	0.3607(1)	0.3608(1)	0.3604(1)
		B/Å^2	0.45(1)	0.40(1)	0.49(1)
Ni	2*a*	B/Å^2	0.32(4)	0.26(4)	0.47(3)
O_I	4*c*	B/Å^2	0.38(11)	0.70(11)	0.76(8)
O_{II}	4*e*	z	0.1689(4)	0.1666(4)	0.1639(3)
		B/Å^2	1.01(11)	0.75(10)	0.95(8)
		R_{wp}	11.57	11.62	10.52
residuals(%)		R_p	8.36	8.28	7.43
		R_e	0.69	0.72	0.67
		R_i	2.95	3.28	3.79

The valence state of nickel in $Sm_{2-x}Sr_xNiO_{4+\delta}$

The mean oxidation number of nickel in the samples is shown as a function of Sr content in Fig. 2. The Ni^{2+} and Ni^{3+}

Table 6 Interatomic distances in $Sm_{2-x}Sr_xNiO_{4+\delta}$

distance/Å	$x = 0.4$	0.5	0.6	0.8	1.0	1.2	Δ (%)
Ni—O_I ($\parallel a$-axis)	1.891(1)	1.885(1)	1.881(1)	1.886(1)	1.892(1)	1.896(1)	0.80
Ni—O_{II} ($\parallel c$-axis)	2.161(6)	2.145(6)	2.119(5)	2.074(5)	2.036(5)	2.000(4)	8.05
Sm—O_{II} ($\parallel c$-axis)	2.272(6)	2.303(6)	2.330(5)	2.355(5)	2.374(5)	2.398(4)	5.55
Sm—O_I	2.554(1)	2.554(1)	2.553(1)	2.546(1)	2.545(1)	2.549(1)	0.35
Sm—Sm ($\parallel c$-axis)	3.435(2)	3.446(2)	3.450(2)	3.421(2)	3.403(2)	3.407(2)	1.38
Sm—Ni ($\parallel c$-axis)	4.433(6)	4.448(6)	4.449(5)	4.429(5)	4.410(5)	4.398(4)	1.16
Ni—O_{II}/Ni—O_I	1.143	1.138	1.127	1.100	1.076	1.055	

Table 7 The average bond valence of Ni, reducing temperature and the sum of the M—O bond formation enthalpies $\Sigma(\Delta H_{M-O})$ in $Sm_{2-x}Sr_xNiO_{4+\delta}$

x	average bond valence of Ni	$T_{max,1}$/K	$T_{max,h}$/K	$\Sigma(\Delta H_{A-O})$/kJ mol^{-1}	$\Sigma(\Delta H_{Ni-O})$/kJ mol^{-1}
0.4	2.62	738	1033	521.2	70.13
0.5	2.68	798	1013	506.3	71.38
0.6	2.74	793	978	491.3	72.62
0.8	2.78	808	1038	461.4	73.45
1.0	2.83	813	1068	431.5	74.48
1.2	2.86	833	1103	401.6	75.10

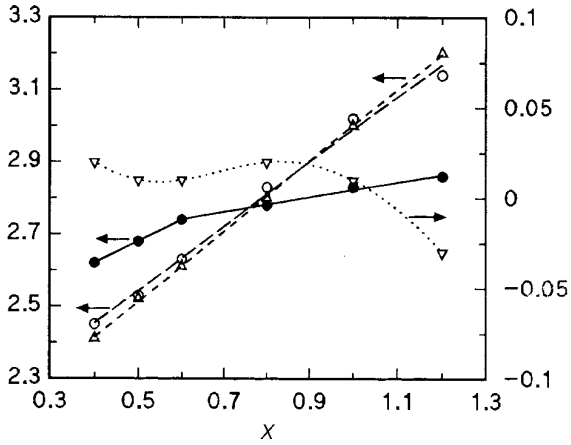

Fig. 2 The average bond valence (●), measured mean oxidation number (○), calculated mean oxidation number (△) of Ni and δ (▽) as functions of x in $Sm_{2-x}Sr_xNiO_{4+\delta}$

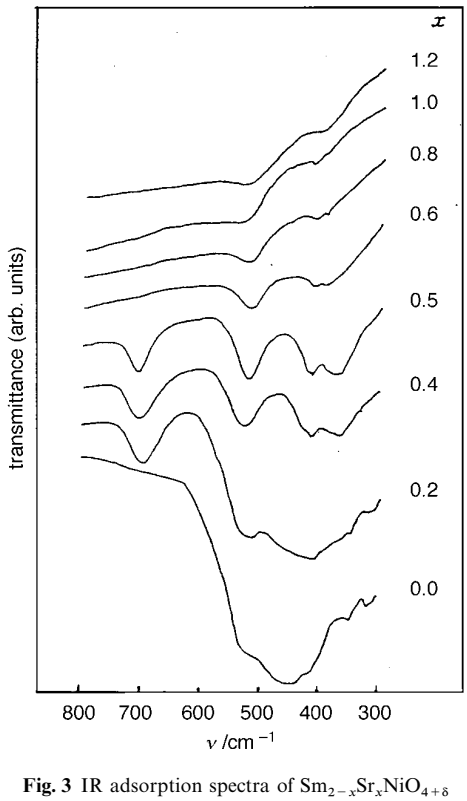

Fig. 3 IR adsorption spectra of $Sm_{2-x}Sr_xNiO_{4+\delta}$

content and the oxygen non-stoichiometry (δ) calculated from the mean oxidation state of nickel, and occupancy (equal to unity), and the formula of $Sm_{2-x}Sr_xNiO_{4+\delta}$ are listed in Table 2. It can be seen that the valence state of nickel in the samples does not deviate much from theoretical data, therefore, the valence state of B ions in A_2BO_4 compounds can be easily controlled by substitution of A ions by A′. In this study, the mean oxidation number of nickel can even be above three (3.02 and 3.14 for $x=1.0$ and 1.2, respectively). These properties should be important in catalysis studies.

Reducibility of $Sm_{2-x}Sr_xNiO_{4+\delta}$

TPR profiles of $Sm_{2-x}Sr_xNiO_{4+\delta}$ are shown in Fig. 4. There are two reduction peaks in the TPR profile for each sample. After the lower temperature reduction, the K_2NiF_4 structure still remains stable although some Ni ions are reduced. The

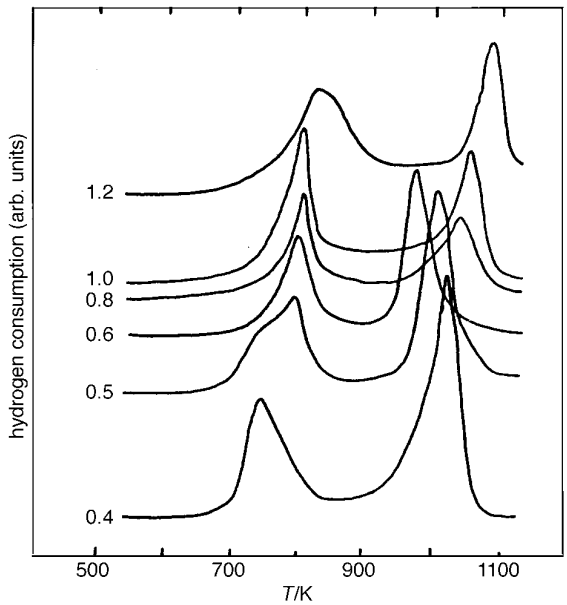

Fig. 4 The TPR profiles of $Sm_{2-x}Sr_xNiO_{4+\delta}$

higher temperature reduction peak leads to total reduction of the sample and the K_2NiF_4 structure is destroyed.[20] The reducibility of the sample is probably determined by the stability of the NiO_6 octahedra in the system. Table 7 lists the reduction peak temperatures (T_{max}) of the peaks and the ratio of the two reduction peaks. The ratio of the peaks is not consistent with the relative amounts of Ni^{2+} and Ni^{3+} in the system, which implies that they do not relate to the reduction of the different valence Ni ions, but rather relate to the reduction of oxygen with different binding energies on different sites. It can then be reasonably presumed that the lower temperature reduction peak is related to the reduction of active O_{II} sites (with longer Ni—O distances and higher thermal factor as indicated in Tables 5 and 6), while the higher temperature peak corresponds to reduction of less active O_I (shorter Ni—O distance and lower thermal factors). In the range $0.4 \leqslant x \leqslant 1.2$, the peak temperature at lower temperature, $T_{max,l}$ increases with x, opposite to the changes of the Ni—O_{II} ($\parallel$ c-axis) distance, and consistent with the average bond valence of Ni. As x increases, $T_{max,h}$ increases in the range $0.4 \leqslant x \leqslant 0.6$, and decreases in the range $0.6 \leqslant x \leqslant 1.2$, which is opposite to the cell parameter c. This means that the structural stability of $Sm_{2-x}Sr_xNiO_{4+\delta}$ is related to the distance between the layers of perovskite and rocksalt.

Conclusion

K_2NiF_4 type samarium nickelate can be synthesized by partial substitution of Sr^{2+} for Sm^{3+} to increase the radius of the A ions and to decrease the radius of B ions by oxidizing the latter into a higher valence state. The Sr^{2+} substitution causes a drastic shift of the O_{II} ions along the c-axis from Sm(Sr) towards Ni whilst scarcely affecting the NiO_4 in the basal plane. The distortion of the NiO_6 octahedron decreases with increasing x from $x=0.4$ to 1.2. The variation with x of the TPR peak temperature is opposite to the variation of the Ni—O_{II} bond length and the cell parameter c, which indicates that the structural stability of $Sm_{2-x}Sr_xNiO_{4+\delta}$ is related to the distance between the layers of perovskite and rocksalt layers.

This study was financially supported by the Natural Science Foundation of Zhejiang Province, China.

References

1 P. Ganguly and C. N. R. Rao, *Mater. Res. Bull.*, 1973, **8**, 405.
2 B. W. Arbuckle, K. V. Ramanujachary, Z. Zhang and M. Greenblatt, *J. Solid State Chem.*, 1990, **88**, 278.
3 B. W. Arbuckle, K. V. Ramanujachary, A. M. Buckley and M. Greenblatt, *J. Solid State Chem.*, 1992, **97**, 274.
4 M. Sayer and P. Odier, *J. Solid State Chem.*, 1987, **67**, 26.
5 C. N. R. Rao, P. Ganguly, K. K. Singh and R. A. Mohan Ram, *J. Solid State Chem.*, 1988, **72**, 14.
6 A. K. Ladavos and P. Pomonis, *J. Chem. Soc., Faraday Trans.*, 1991, **87**, 3291.
7 T. Nitadori, M. Muramatsu and M. Misono, *Bull. Chem. Soc. Jpn.*, 1988, **61**, 3831.
8 A. Albinati and B. T. M. Willis, *J. Appl. Crystallogr.*, 1982, **15**, 361.
9 Y. Takeda, R. Kanno, M. Sakano, O. Yamamoto, M. Takano, Y. Banndo, H. Akinaga, K. Takita and J. B. Goodenough, *Mater. Res. Bull.*, 1990, **25**, 293.
10 H. Zheng, S. Du, G. Lu, H. Lou and F. Ma, *Acta Chim. Sinica*, 1993, **51**, 373.
11 Y. Takeda, M. Nishijima, N. Imanishi, R. Kanno, O. Yamamoto and M. Takano, *J. Solid State Chem.*, 1992, **96**, 72.
12 D. Ganguli, *J. Solid State Chem.*, 1979, **30**, 353.
13 A. Sakthivel and R. A. Young, *User's Guide to Programs DBWS-9006*, 1981.
14 B. E. Gushee, L. Katz and R. Ward, *J. Am. Chem. Soc.*, 1957, **79**, 5061.
15 A. Jones and B. D. McNicol, *Temperature-Programmed Reduction for Solid Materials Characterization*, Dekker, New York, 1986, p. 105.
16 R. D. Shannon, *Acta Crystallogr., Sect. A*, 1976, **32**, 751.
17 A. K. Ladavos and P. J. Pomonis, *Appl. Catal. B*, 1992, **1**, 101.
18 I. D. Brown and K. K. Wu, *Acta Crystallogr., Sect. B*, 1976, **32**, 1957.
19 K. K. Singh, P. Ganguly and J. B. Goodenough, *J. Solid State Chem.*, 1984, **52**, 254.
20 H. Lou, F. Ma and Y. Chen, *React. Kinet. Catal. Lett.*, 1990, **42**, 151.

Paper 7/03271D; *Received* 12*th May*, 1997